MECHANISTIC DESCRIPTION, SIMULATION, AND INTERPRETATION OF SPONTANEOUS POTENTIAL LOGS

Joshua Bautista-Anguiano and Carlos Torres-Verdín, The University of Texas at Austin

This paper was prepared for presentation at the SPWLA 56th Annual Logging Symposium held in Long Beach, California, USA, July 18-22, 2015.

ABSTRACT

Spontaneous Potential (SP) and Gamma Ray (GR) logs are often the only measurements available in many old hydrocarbon fields. Reliable coupled petrophysical interpretation of GR and SP logs requires previous accurate quantitative calibration for the effects of shale laminations, water electrolyte concentration, temperature, bed thickness, borehole diameter, hydrocarbon saturation, and invasion, among others. Although the latter effects on SP logs are well known, there is no published numerical algorithm that quantifies the relative contributions of all geometrical, petrophysical, and fluid effects on SP logs.

This paper develops a new mechanistic description of SP logs for their numerical modeling and petrophysical interpretation in vertical wells penetrating horizontal layers. The main objective of the new SP modeling method is to estimate water saturation reliably in wells where only SP and GR logs are available but where resistivity and porosity calibrations can be performed in a key well within the same field or can be inferred from core data.

The mechanistic SP modeling algorithm is based on the fundamental concept of anion and cation migration in aqueous solutions with unequal electrolyte concentration via diffusion and membrane potentials. It explicitly accounts for specific borehole conditions, temperature, variable shale properties, finite bed thickness, shale laminations, hydrocarbon saturation, and invasion (including salt concentration profiles) in the numerical modeling of SP logs. Further, hydrocarbon saturation effects on SP logs account for the rock's effective throat radius. Sensitivity studies are carried out to quantify selectively the effect of each environmental and geometrical variable on measured SP logs. The modeling algorithm is also successfully used to reproduce SP logs acquired in the presence of salt and water saturation fronts in invaded hydrocarbon-saturated rocks. Examples of application include sandstone sequences that have internal shale laminations.

INTRODUCTION

The Spontaneous Potential (SP) log has been a source of information used by generations of log analysts for the identification of permeable beds in siliciclastic sedimentary sequences. Work toward the identification of the effect of hydrocarbons with the aid of the SP log was published several decades ago (Doll, 1949, Poupon et al., 1954, Waxman and Smits, 1968). However, to the authors' knowledge, no previous numerical modelling algorithms and interpretation methods have been documented in the open technical literature where water saturation as well as other factors that affect the SP log are simultaneously taken into account.

A first attempt to describe the physics behind the SP log was made by Doll (1949). However, given the work published by Woodruff et al. (2010) and Revil (1999), part of the theory published in the classic work from Doll (1949) cannot be proven or is inaccurate. Our work, as does the work by Woodruff et al. (2010), attempts to clarify the physics of the SP log and to encourage people to abandon the old models based on Doll (1949) and replace them with more accurate models.

"SP suppression", as defined in several studies (Poupon et al., 1954, Kerver and Prokop, 1957, McCall et al., 1971), is the reduction in the amplitude of the deflection in the SP log due to hydrocarbon content. However, bed thickness, formation invasion, and shale laminations have a similar effect, making it difficult to qualitatively determine potential hydrocarbon zones. This makes the interpretation of the SP log cumbersome and unreliable if all these factors are not considered simultaneously.

We document a sensitivity analysis of all the factors mentioned above related to the SP amplitude. These factors are considered in the forward simulation of two field cases of laminated sandstones, to which we will refer as Case I and Case II. We explain how the SP log

can be simulated and how a mechanistic description that takes into account the effects of shale, bed thickness, temperature, ion migration, and hydrocarbon saturation can be used in conjunction with other conventional logs. This work is performed by constructing an earth model that yields an appropriate match for other logs (nuclear and resistivity logs). Once these logs are matched and the earth model properties fixed, the distribution of water, salinity, bed thickness, temperature, and shale content are used in conjunction with our SP petrophysical model to simulate the SP log and compare it to field measurements.

Case II in particular shows an anomalous SP behavior that does not correlate with other logs. The development of our petrophysical model is still insufficient for an appropriate simulation of the SP log in this case. However, we provide a mechanistic explanation for the anomalous behavior, which could be extended to similar cases in other fields.

The final goal of our work is to verify that the SP log forward simulation, when properly calibrated, could allow the interpretation and definition of hydrocarbon zones where only SP and Gamma Ray (GR) logs are available, based on a key well with abundant information about the reservoir under examination.

Our work is based on the following assumptions:

- The well and beds are vertical and horizontal, respectively.
- The only salt dissolved in water is NaCl.
- Only the electrochemical component of the SP log is measured.
- The formation is water wet. This is equivalent to assuming that water in the rock is topologically connected.
- The electrokinetic component of the SP is negligible.

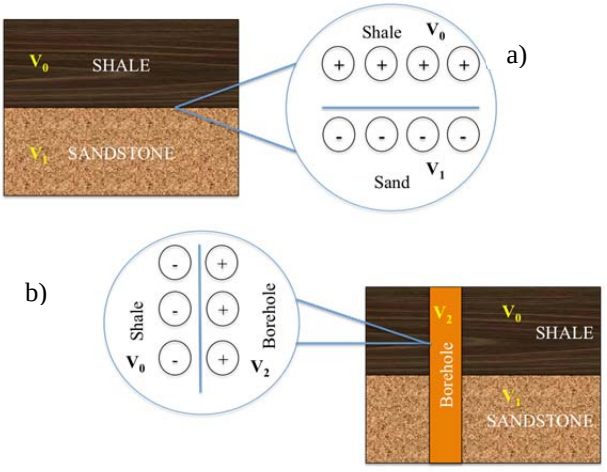

Figure 1. Schematic representation of the double layer of ions at the interface. a) Double layer at the sandstone-shale interface. b) Double layer at the borehole-shale interface.

THEORETICAL BACKGROUND

The SP log has its origin from spontaneous electrical sources, which are any ion transport process in nature capable of causing a long-term charge separation, i.e., for a period of time long enough to be measured and recorded. From all the ion transport processes in nature, the transport of ions across a charged membrane is capable of generating a measurable signal of electric potential (Mounce and Rust, 1944, Doll, 1949, Hill and Milburn, 1956, Revil, 1999). Shale beds are naturally charged membranes (Revil, 1999, Meunier, 2005). If a gradient of concentration (more properly, activity) of ions exists between the fluid of an uncharged porous medium (i.e., a sand bed) and the charged porous medium (i.e., a shale bed), ions migrate in the opposite direction of the gradient of concentration. However, given the inherent charge in the pore network in one of the media, the coions (Revil, 1999) do not migrate, or at least are retarded, opposite to the gradient. This behavior results in charge separation, having negative charges on one side of the boundary between the porous media, and positive ones on the other. The negative charge accumulates and attracts cations back, moving them with the gradient of concentration. At steady state, a double layer of ions forms at the boundary, with the same

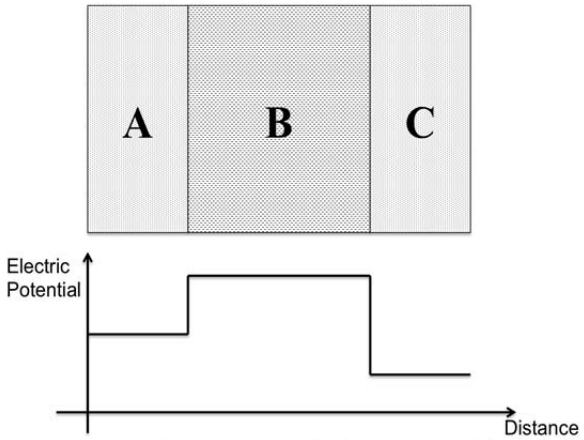

Figure 2. Schematic representation of electric potential discontinuities that occur in media *A*, *B* and *C*, due to the inherent charge of medium *B*. *B* is assumed to be a perfect membrane, meaning that no negative ion can pass through it. This generates charge separations at the interfaces *A*-*B* and *B*-*C* and gives rise to potential discontinuities.

amount of positive ions leaving and entering the charged medium, thus giving rise to a net ionic current of zero (Revil, 1999). Given this double layer at the boundary, an electric potential discontinuity occurs (Eskola, 1992), which causes the deflections in the SP log measured in a well.

The mathematical expression that relates the gradient in the electric potential to the gradient in concentration is given by Revil (1999) as

$$\nabla V = -\frac{k_b T}{e}\left(2t_{Na}^{f} - 1\right)\nabla \ln\left(\sigma_f\right) \qquad (1)$$

In Eq. (1) V is electric potential, k_b is Boltzmann's constant, T is absolute temperature, e is elementary charge, t_{Na}^{f} is transport number of sodium in water and σ_f is electrolyte conductivity. In Eq. (1) we make the same assumptions made by Revil (1999).

Equation (1) is a vectorial equation, which relates the gradient in concentration to the gradient in electric potential. Solving a vectorial equation can be complicated, given that it must be solved for all the components of the vector. In order to simplify the solution, the divergence operator is applied on both sides, namely,

$$\nabla^2 V = \nabla \cdot \left(-\frac{k_b T}{e}\left(2t_{Na}^{f} - 1\right)\nabla \ln\left(\sigma_f\right)\right) \qquad (2)$$

In Eq. (2) there is no dependency on conductivity, contrary to what is stated by Doll (1949) or Tabanou et al. (1988). The electrochemical component of the SP is not affected by the resistivity of the formations.

Figure 1a shows a set of beds before being drilled. At the interface between the beds there is a discontinuity in electric potential. This double layer of ions must not be confused with the electrical double layer that exists at the surface of mineral grains; it is a dynamic double layer: ions migrate from one medium to the other, reaching a dynamic equilibrium at steady state where surface charge density remains constant. Once the well is drilled, new double layers form at the contact surfaces of the wellbore with the beds, giving rise to a new configuration of the electric potential field (**Figure 1b**), which is what is measured.

The variable that captures the link between the SP log and petrophysics is found in the transport number t_{Na}^{f} of sodium in Eq. (2). The transport number is a non-

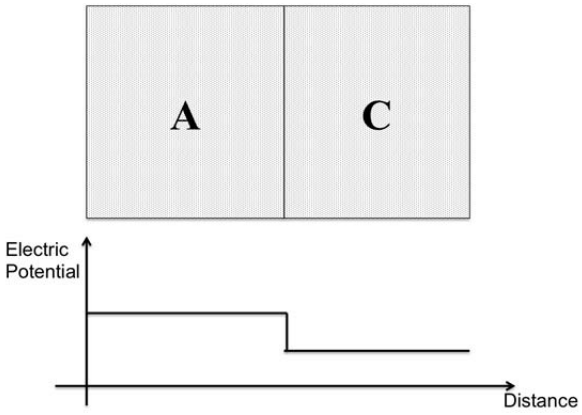

Figure 3. Schematic representation of the potential discontinuity generated in this case is due to the difference in mobility between chlorine and sodium.

dimensional representation of the relative mobility of each ion. This number can take values between 0 and 1. In water, for example, sodium has a transport number approximately equal to 0.38, while chlorine ions have a transport number of 0.62 (Revil, 1999). Such a behavior indicates that chlorine ions diffuse 1.56 times faster than the sodium ions in water.

For naturally charged membranes, such as shale beds, chlorine ions are mostly prevented from diffusing because of electric repulsive forces from the membrane. This makes the mobility of chlorine ions inside the shale bed close to zero. In the case of sandstone or limestone formations, the surface of the solid framework of the rock is also naturally charged, but because of relatively large pore and pore-throat sizes in such rocks, compared to the pores of shale beds, the electric repulsion has no significant effect on ion migration. Hence, chlorine ions can move with no restrictions along the center of the pores, away from the solid matrix where the electrical double layer exists. As water saturation decreases, the space available for chlorine ions to move is reduced, reaching the order of magnitude of the electric double layer. Therefore, electric repulsive forces have a significant effect on the movement of chlorine ions, as explained by Kerver and Prokop (1957).

Figure 2 shows the response when a double layer forms at both sides of the negatively charged membrane *B*. Consequently, *A*, *B* and *C* will be at different electric potentials, given that these potentials remain constant inside each subdomain. Two attending remarks can then be made:

1. Regardless of the salinity of the water inside membrane *B*, the difference in the electric potential between media *A* and *C* remains constant, as long as *A* and *C* have no changes in the salinity of the water they contain.

2. The potential difference between *A* and *C* is known as the membrane potential.

Since the work by Doll (1949), the term "SP current" has been widely used in the well logging literature. Such current does not exist for the electrochemical component of the SP log. The origin of SP phenomena is the charge separation that occurs because of the different mobilities ions have and not a current as suggested by Doll (1949).

In **Figure 3** no membrane exists between *A* and *C*. A double layer forms as well, since now chlorine is free to move and advances ahead of sodium 1.56 times faster. This gives rise to diffusion or liquid-junction potential. The charge separation in this case, contrary to what happens with a charged membrane, disappears with time given that complete diffusion can occur between *A* and *C* (Mounce and Rust, 1944). When *A* and *C* reach a concentration equilibrium, there will be no difference in their electric potentials.

Electrochemical and Electrokinetic Components.

From the work by Woodruff et al. (2010), a more general expression for the SP is

$$\nabla \cdot \boldsymbol{j} = \nabla \cdot \left(-\sigma \nabla V + \frac{Q_v}{S_w} \boldsymbol{u} - \frac{k_b T}{e} \left(2t_{Na}^f - 1\right) \sigma \nabla \ln(\sigma_f) \right) \qquad (3)$$

In Eq. (3) σ is rock's conductivity, Q_v is excess charge per unit pore volume, and $\boldsymbol{u}$ is Darcy velocity of the electrolyte. At steady state conditions, $\nabla \cdot \boldsymbol{j} = 0$. From Eq. (3) it is possible to prove that the electrochemical component of the SP is independent of the conductivity of the media, while the electrokinetic component depends on it.

It is possible to rewrite Eq. (3) as

$$\begin{gathered} -\sigma \nabla^2 (V_{EK} + V_{EC}) - \nabla \sigma \cdot \left(\nabla V_{EK} + V_{EC} + \right. \\ \left. K \nabla \ln \sigma_f \right) + \nabla \left(Q_v \right) \cdot \boldsymbol{u} - \nabla K \cdot \left(\sigma \nabla \ln \sigma_f \right) - \\ \sigma K \nabla^2 \ln \sigma_f = 0 \,, \end{gathered} \qquad (4)$$

where $V = V_{EK} + V_{EC}$ and $K = \frac{k_b T}{e}\left(2t_{Na}^f - 1\right)$; V_{EK} and V_{EC} are the electrokinetic and electrochemical components of the SP log, respectively. Considering from Revil (1999), that $\nabla V_{EC} + K \nabla \ln \sigma_f = 0$, Eq. (4) can be rewritten as

$$\begin{gathered} \sigma \nabla^2 (V_{EK} + V_{EC}) + \nabla \sigma \cdot \nabla V_{EK} - \nabla (Q_v) \cdot \boldsymbol{u} + \\ \sigma \left(\nabla K \cdot \nabla \ln \sigma_f + K \nabla^2 \ln \sigma_f \right) = 0 \end{gathered} \qquad (5)$$

By separating the EK and EC components in Eq. (5), and considering that the superposition principle applies for the SP phenomenon (Woodruff et al., 2010), we obtain

$$\nabla \cdot (\sigma \nabla V_{EK}) = -\nabla \left(Q_v \right) \cdot \boldsymbol{u} \qquad (6)$$

$$\nabla^2 V_{EC} = -\nabla \cdot \left(\frac{k_b T}{e} \left(2t_{Na}^f - 1\right) \nabla \ln \sigma_f \right) \qquad (7)$$

Equation (6), which describes the electrokinetic component of the SP log, clearly depends on conductivity, as is shown in Bolève et al. (2007). On the other hand, Eq. (7) has no dependence on conductivity. For this work, we only consider the electrochemical component of the SP.

Proposed Petrophysical Model for SP Log Modeling.

The petrophysical model proposed for this work is shown in Eq. (8) and is based on a parallel-circuit analogy, as shown in **Figure 4**, namely,

$$t_{Na}^{eff} = \left(\left(1 - \frac{B}{S_w}\right) t_{Na}^f + \frac{B}{S_w} t_{Na}^s \right) (1 - A) + A t_{Na}^{sh} \,, \qquad (8)$$

where:

A = Parameter that indicates the fraction of ions that move through shale/clay in a rock. This is equivalent to the volumetric concentration of shale for laminated sequences.

B = Parameter that relates the double-layer thickness on the mineral grains to the pore throat size.

S_w = Non-shale/clay water saturation.

t_{Na}^{sh} = Transport number of sodium ions through the shale/clay. For a perfect membrane, $t_{Na}^{sh} = 1$, membrane efficiency is 100%.

t_{Na}^{s} = Transport number of the sodium ions in the diffuse double layer region. If only sodium ions can migrate in this region, $t_{Na}^{s} = 1$.

t_{Na}^{eff} = Effective transport number of sodium in the rock.

If a rock has no clay/shale, parameter A is zero and the effective transport number depends on the transport number in bulk water t_{Na}^{f} and parameter B. If no double layer exists, then B is zero and the SP amplitude is independent of the water saturation. This does not take into account percolation thresholds for water saturation and effective porosity, since in this model the aqueous phase remains topologically connected and there is always a path for ions to migrate. For Case II (see *Results: Field Cases*), the same behavior does not take place and the model is not completely accurate for modeling purposes. However, it is included in this work to show that the explanation for such a case can be provided from the mechanistic approach presented here.

Parameter A can take into account the topology of the shale/clay as shown in Eq. (9). In this equation, laminated or dispersed topologies are considered. For a laminated system $V_{disp} = 0$, leaving parameter $A = V_{sh}$, i.e.,

$$A = V_{sh}\left(1 - V_{disp}\right) + \frac{V_{sh}}{\phi_s} V_{disp}\,, \qquad (9)$$

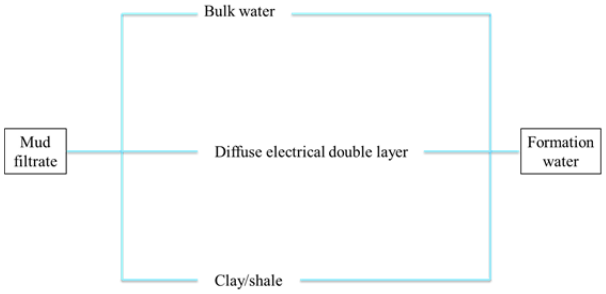

Figure 4. Ions can follow one of the three paths shown when they migrate. For the model developed in this work, this is considered to be a parallel-circuit analogue, from which Eq. 8 is developed. Depending on which path predominates, it is the SP signal that will be measured in the borehole.

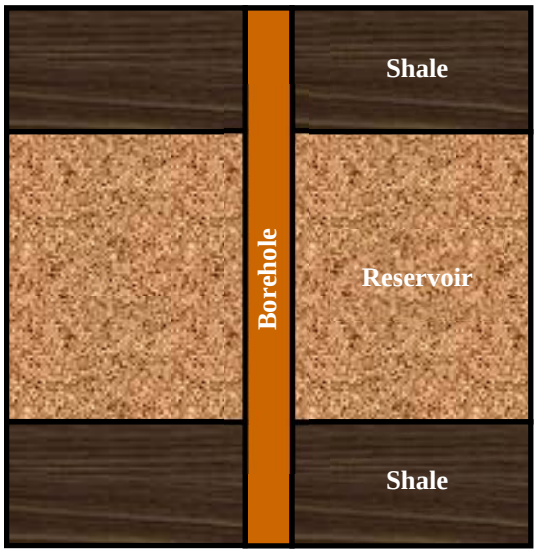

Figure 5. Schematic representation of the model used for the sensitivity analysis. The model consists of three horizontal beds and a vertical well.

where V_{sh} is volumetric concentration of shale/clay, V_{disp} is fraction of shale/clay that exists dispersed in the pore network, and ϕ_s is total porosity.

For parameter B, the following ratio is introduced:

$$B = \frac{DL}{PT}\,, \qquad (10)$$

where DL is electrical double layer thickness, considered to be the Debye length, and PT is pore radius.

Equation (10) assumes that the pore network is a bundle of cylindrical tubes whose radius is constant. For a rock with relatively large pores, parameter B is small, meaning that most of sodium ions travel in the bulk water. If the electrical double layer is of the same order of magnitude as the pore radius, parameter B would be relevant in the effective transport of ions, since more sodium than chlorine ions migrate, giving rise to a charge separation. This model does not consider electrical double layer overlap.

When the rock has a pore throat size distribution, a way to calculate an effective parameter B_{eff} is

$$B_{eff} = \sum_i^M V_i B_i\,, \qquad (11)$$

where:

B_i = B parameter for a particular pore throat size.

V_i = Volume fraction of the pore space for that particular pore size.

M = Total number of pore-throat sizes.

SENSITIVITY ANALYSIS

In this section, different factors that alter the amplitude of the SP log are examined and sensitivity analysis curves obtained from Equations (2) and (8) for a synthetic three-layered model: one reservoir (i.e., sandstone) bed shouldered by two shale beds, as shown in **Figure 5**.

Numerical simulations were carried out using a finite-difference representation of Eq. (2) in cylindrical coordinates with a regular, equally spaced mesh, and with no-flow boundaries at the termination of the mesh.

Figure 6 describes the variation of the SP amplitude as a function of normalized bed thickness. Values are obtained for a reservoir with $S_w = 1.0$, shale free, no invasion present, and no effects of the electrical double layer. The behavior of the SP amplitude is consistent with results documented in Doll (1949).

Figure 7 shows the effects on the SP log amplitude with respect to volumetric concentration of shale. For the laminated case, V_{sh} varies from 0 to 1. For the dispersed case, V_{sh} varies from 0 to 0.3 because the rock modelled was given a value of total porosity of 0.3. The total porosity and effective porosity are considered the same for this model. In cases where effective porosity is smaller than the total porosity, the curve for dispersed shale would be expected to exhibit a larger slope.

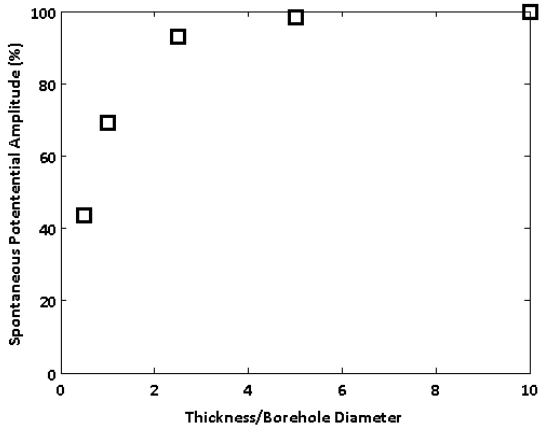

Figure 6. Bed thickness effect on the SP amplitude.

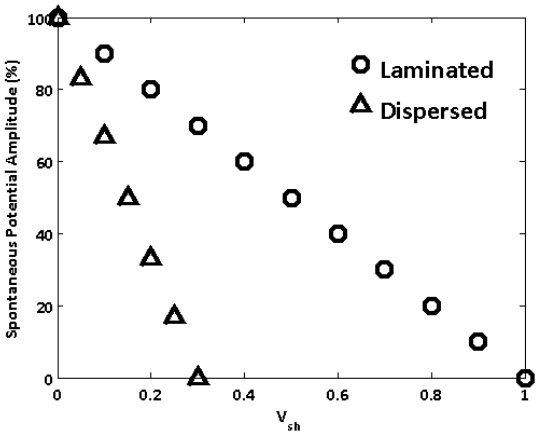

Figure 7. Effect of volumetric concentration of shale as laminations or dispersed on the SP amplitude.

Figure 8 and **Figure 9** show the SP behavior as water saturation and pore size varies for a clean formation. The trend of these plots follows the experimental results from Kerver and Prokop (1957). From such predictions, we would expect that for rocks with large pores, relative to the electrical double layer thickness, the SP amplitude would vary rapidly at values below 20% of water saturation. The rock simulated is assumed shale/clay free in this case.

In **Figure 8**, each curve results from different values of B. Adjusting this parameter is a key step in order to properly calibrate and simulate the SP log and properly estimate water saturation. This is because reservoirs with high hydrocarbon saturation (low S_w) are expected to be have a larger impact on the SP log than reservoirs with high values of S_w. However, pore-throat size needs

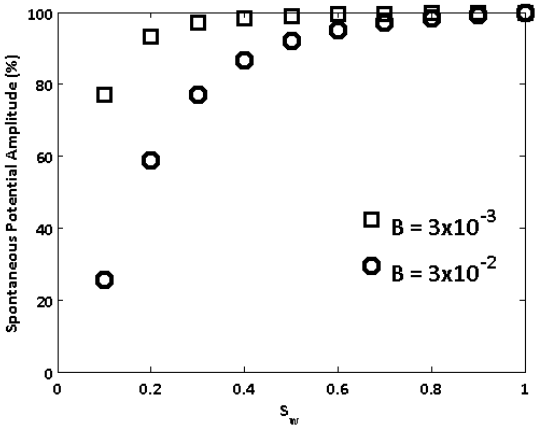

Figure 8. Effect of water saturation on the SP amplitude as predicted by the petrophysical model proposed in this paper.

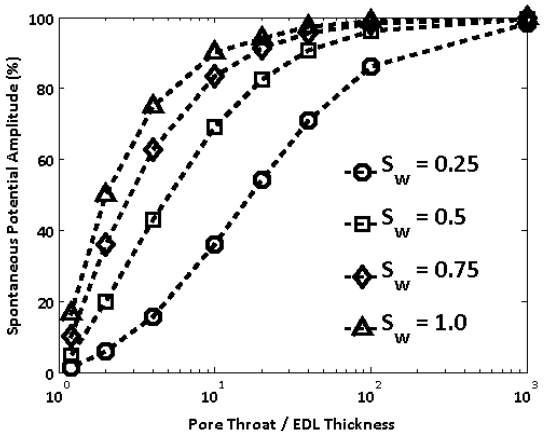

Figure 9. Pore-throat size. For a rock with different values of water saturation, the SP amplitude varies as the pore size becomes smaller.

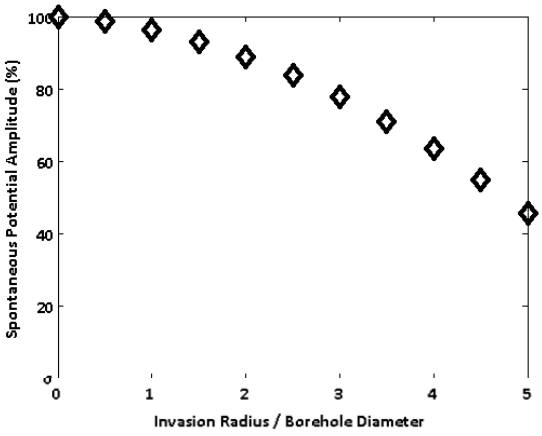

Figure 10. Radius of invasion. This plot shows the behavior of the SP amplitude for a piston-like invasion front.

to be carefully taken into account because a reservoir with small pore throats and high S_w values can yield an SP signal similar to that of a reservoir with low S_w and larger pore throats.

Figure 10 shows the SP amplitude as a function of invasion radius for a clean water-saturated formation. As invasion radius grows, the SP amplitude decreases, as observed in the field. This figure assumes a piston-like profile for salinity and water saturation, hence it should be considered with care because this is not a general field condition.

RESULTS: SYNTHETIC CASES

Two synthetic cases are examined and compared in **Figure 11**. These synthetic cases are composed of alternating beds of sandstone and shale, each 5 ft thick. In **Figure 11a**, bed (2) is a sandstone that has shale laminations equivalent to V_{sh} = 0.2 and has S_w = 0.3 in the sandstone laminations. Water saturation increases downward, as would be expected in any real case. The difference between **Figures 11a** and **11b** is the presence of laminations of shale in bed (2). **Figure 11b** shows the response of the SP log for bed (2) with no shale laminations. As can be observed, without laminations the simulation yields a very similar response to bed (4),

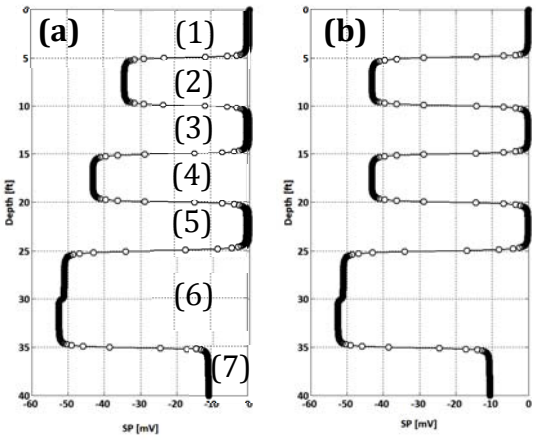

Figure 11. Synthetic cases. (a) Bed 2 with shale laminations equivalent to V_{sh} = 0.2 and (b) Bed 2 without shale laminations.

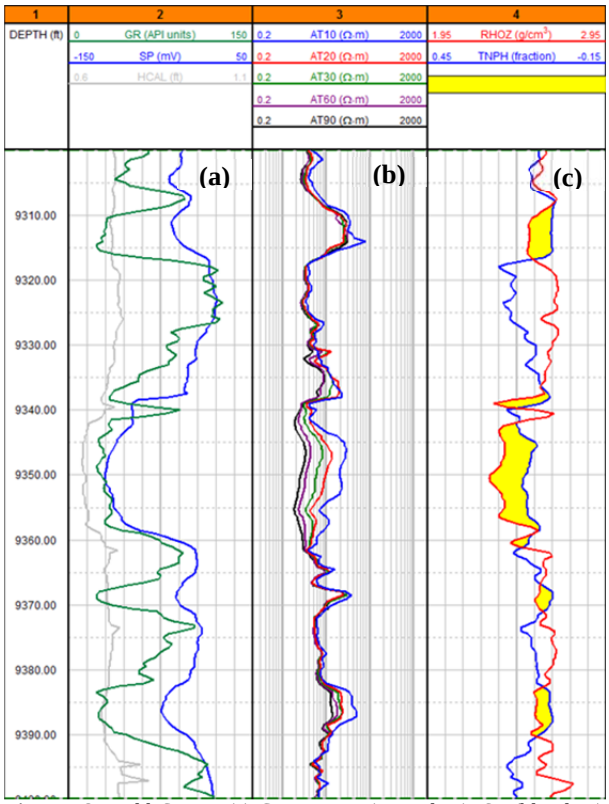

Figure 12. Field Case I. (a) Gamma-ray (green line), SP (blue line) and Caliper (gray line) logs, (b) induction resistivity logs, (c) neutron and density logs in limestone units.

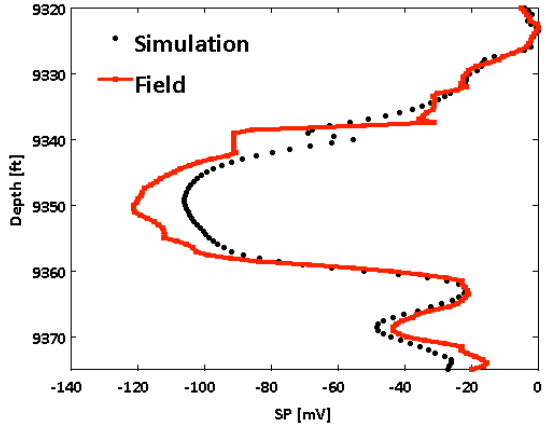

Figure 13. Comparison between field and numerically simulated SP logs for Case I.

which has S_w = 0.6 and V_{sh} = 0.2. This exercise confirms that the algorithm employed reliably reproduces the relative contributions of shale lamina, borehole size, water saturation, and salt concentration altogether, following the sensitivity analysis curves documented in the previous section.

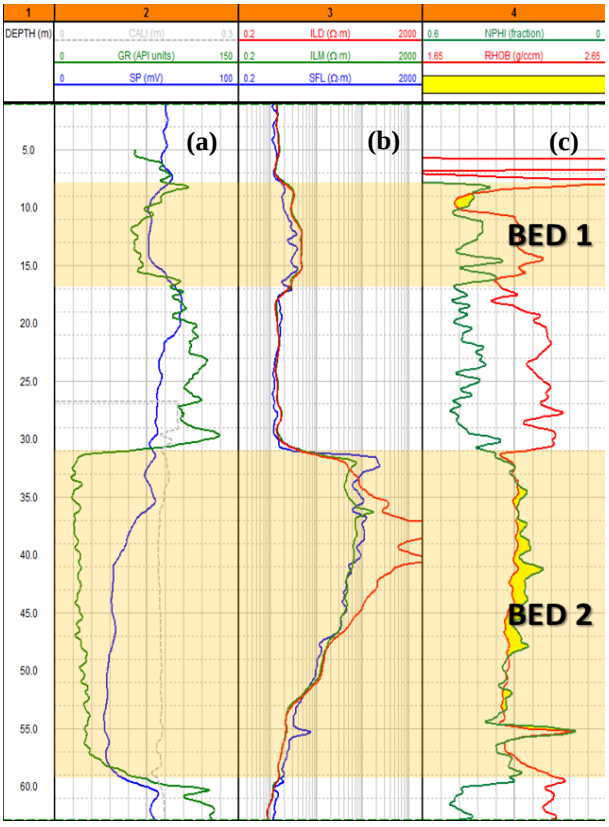

Figure 14. Field Case II. (a) Gamma ray (green line), SP (blue line), and Caliper (gray line) logs,(b) induction resistivity logs, (c) neutron and density logs in sandstone units. Two sandstone layers can be identified from the gamma-ray log. A loss in amplitude in the SP log can be observed at the top of Bed 2.

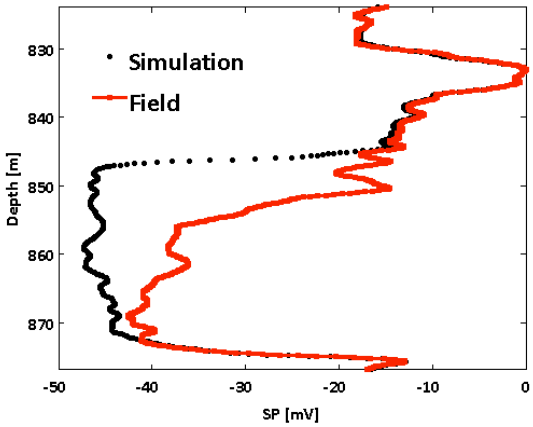

Figure 15. Comparison between field and numerically simulated SP logs for Case II.

In **Figure 11**, bed (7) is a leaky shale bed wherein the sodium transport number is equal to 0.9, meaning that a small fraction of chlorine ions can migrate. As expected, the SP along the leaky shale does not return to the shale baseline.

Bed (6) in Figure 11 shows a sharp transition between S_w = 0.8 and S_w = 1.0, with V_{sh} = 0.2. Capillary pressure is not considered in this case, but it can be taken into account if water saturation is known as a function of depth.

The above synthetic cases were constructed with no invasion included in permeable formations. They were also constructed with thick enough beds so that they will attain their maximum SP amplitude in order to compare results to the classical analysis introduced by Poupon et al. (1954) below.

Recalling the work of Poupon et al. (1954), the SP response that would be expected is given by

$$PSP = -M\log\frac{R_{xo}}{R_t} - 2\alpha M\log\frac{S_{xo}}{S_w}, \qquad (12)$$

where PSP is the SP amplitude for a laminated shaly sand, M is a coefficient between 60 and 80 [mV] according to Poupon et al. (1954), R_{xo} is the resistivity of the flushed zone, R_t is the resistivity of the virgin zone, S_{xo} is the water saturation of the flushed zone, S_w is the water saturation of the virgin zone, and α is a reduction factor.

Without invasion (or negligible invasion), Eq. (12) yields $PSP = 0$, which is not correct. This is a problem recognized in Poupon et al. (1954), since layers with $S_w = S_{xo}$ would be indeterminate by the fact that $PSP = 0$ is not what is observed in the field. Their method relies on the adequate determination of α, for which no method is provided for its estimation. It should also be remarked that this α factor is not affected by bed thickness, pore-throat size or leaky shales, which are not uncommon in field cases. Our algorithm, on the other hand, does not rely on Archie's equation, which is empirical, and no emprirical estimation for α is necessary. We assume a variable K according to temperature, the membrane efficiency, pore- throat size, and water saturation for a water-wet medium.

RESULTS: FIELD CASES

Case I: North Louisiana Tight Gas Sand Formation

This formation consists of fine- to very fine-grained sandstone, shale, and some sandy, fossiliferous oolitic limestone. Interpretation of a large area of the formation suggests global sediment deposition by a system of coalescing deltas prograding from the west, northwest, and north (Finley et al., 1984, Salazar et al., 2006).

We selected a section of 55 ft of measured depth to simulate the SP log. **Figure 12** shows the available logs used to create an earth model and simulate the SP log.

An earth model was constructed with static and dynamic reservoir properties that would match the measured logs, with the help of The University of Texas at Austin's Petrophysical and Well-Log Simulator (UTAPWeLS). Once this earth model honored the available well logs as closely as possible, the resulting water saturation and salinity profiles, and volumetric concentrations of shale/clay were used as the input information for SP log simulation. **Figure 12** compares the measured log and the simulated one. It can be observed that the simulation result is accurate in most of the depth section, especially given that there are several variables that need to be constrained in order to accurately simulate the SP log. The only discrepancy is found at a depth of approximately 9340 ft, which cannot be explained with the information available.

Because this is a tight formation given the low values of permeability (~0.1 md), electrokinetics can be neglected,

Case II: West-Emsland Sandstone (Germany)

The second case was provided to us by Wintershall because of the anomalous behavior in the SP log. We believe that it is worth showing the analysis made in this case in order to verify our mechanistic approach.

Figure 14 shows the field logs. These logs were acquired in a siliciclastic sequence with shale laminations and shale beds. Two sandstone beds can be identified from the GR log, which we have designated as Bed 1 and Bed 2. Our analysis is focused on Bed 2.

An earth model was built with UTAPWeLS, matching the nuclear and resistivity logs as well as possible. Even though we obtained a realistic earth model that matched the nuclear and resistivity logs, it was not complete enough to match the SP log, as shown in **Figure 15**. An interpretation of this case is given in the Discussion section, where the wettability of this formation is taken into account to explain the unexpected results.

At the top of Bed 2, we have a decrease in the SP amplitude which cannot be due to thickness because this bed is several meters thick. The GR log and core samples also reveal that the formation is clean. At first we assumed that pore-throat size could be causing this sudden change in the SP. However, after examining the granulometric measurements provided by Wintershall and having estimated the pore-throat size from well tests and the Kozeny-Carman model, we obtained a value of B that yielded a simulated SP close to that measured in the well, but only if water saturation values were below 1%. Pores are several orders of magnitude larger than the electrical double layer, as would be expected from a reservoir with an average permeability of 13,000 mD. Therefore, the water saturation necessary would be expected to be of that below 1%. In reality, water saturation is never less than 4%. In the next section, we provide an explanation for this case.

DISCUSSION

As observed in **Figure 13**, the simulation for Case I yields a good match with the field log. Simulation results were obtained by taking into account that the formation is tight and that pore throats are in the order of the electrical double layer thickness ($B = 0.65$). Without any other source of information, this is the main assumption made in order to arrive at the results shown in Figure 13.

The pore-throat distribution at each depth, as well as the thickness and influence of the electric double layer, represent properties that need to be measured in order to accurately and reliably simulate the SP log. Without those properties, only educated guesses can be made, based on the salinity of the formation, its wettability, and its permeability, if any of these factors are known.

Shales are considered to be perfect membranes, allowing solely the flow of positive ions. For Case I, shales were considered perfect membranes. Without specific knowledge about shale membrane efficiency and composition (30% illite) this is the best approximation that could be obtained.

For Case II, we observed that the simulated logs did not match Bed 2 of the reservoir. Our explanation is the fact that our model assumes that the aqueous phase (i.e., formation water) is topologically connected, enabling ions to migrate to or from the borehole. However, we were informed by Wintershall that sandstones in this reservoir are oil-wet and can reach values of water saturation as low as 5%. From such an observation, we believe that the reason why the SP log decreases so suddenly is that a threshold in water saturation is reached at which the aqueous phase stops being topologically connected at the top of the reservoir. It follows from this observation that no ion exchange can occur between the borehole and the formation. Such a behavior yields a SP response as if formation water and mud filtrate had the same salinity, despite the fact that this not the case.

In order to obtain a good match in the remaining depth zones, the shale in this reservoir was assigned a sodium transport number of 0.72 (shales in this reservoir are not expected to be perfect membranes).

Fields analogous to the Case II could occur in other parts of the world. To the authors' knowledge, no published work has addressed similar interpretation problems. Therefore, this example sets the path for further research on oil-wet formations and their relationship to the SP log.

CONCLUSIONS

A new model was introduced to quantify the behavior of SP under different petrophysical conditions and that reproduces previous observations and measurements. To the authors' knowledge, this is the first open publication which advances a mechanistic procedure to simulate SP logs by simultaneously accounting for different geometrical and petrophysical factors.

Water saturation cannot be reliably estimated if wettability, permeability, and invasion radius are taken into account in the SP log simulation. With the introduced model, reliable water saturation still cannot be made solely from the SP log.

The mechanistic approach proposed here is limited to reservoirs where formation water is topologically connected, which makes it not applicable to situations where the physics of the reservoir is ruled by percolation thresholds. However, the same mechanistic approach can be extended to study reservoirs where formation water is not a continuum. Further research is needed to include percolation thresholds in ion exchange phenomena.

We documented two cases in which the simulation of the SP log was verified with the current limitations of the model. However, the SP log analysis, when properly implemented in conjunction with other logs in a key well, can be used for identification of potential hydrocarbon zones that might have been overlooked in the past in old wells. This can be done if enough information about the reservoir is available from the key well or from core data for proper calibration of the SP model.

The most challenging step in SP log simulation is the proper petrophysical description of the formation, taking into account wettability, pore-throat distribution in porous media, shale membrane behavior and topology, and salt composition. This information is not readily available in all cases; assumptions might be necessary.

Invasion depth is crucial information for the SP log simulation in old wells. Lack of data on invasion depth could prevent the correct estimation of water saturation, especially when no additional information beyond the SP and GR logs is available. Even with knowledge of petrophysical properties of formations in the same reservoir, invasion depths could be different from well to well in the same reservoir. More research is needed to overcome this obstacle.

ACKNOWLEDGEMENTS

The work reported in this paper was supported by the University of Texas at Austin's Joint Industry Research Consortium on Formation Evaluation, supported by

Afren, Anadarko, Aramco, Baker-Hughes, BG, BHP Billiton, BP, Chevron, China Oilfield Services Ltd., ConocoPhillips, Det Norske, ENI, ExxonMobil, Halliburton, Hess, Maersk, Paradigm, Petrobras, PTT Exploration and Production, Repsol, RWE, Schlumberger, Shell, Southwestern Energy, Statoil, TOTAL, Weatherford, and Wintershall and Woodside Petroleum Limited.

Financial support was provided by the Education Ministry (SEP) of the Mexican Government in the form of a partial fellowship bestowed to Joshua Bautista-Anguiano.

A note of special gratitude goes to Wintershall for granting permission to use their data and ancillary information in this work.

REFERENCES

Bolève, A., Revil, A., Janod, F., Mattiuzzo, J. L., and Jardani, A., 2007, Forward modeling and validation of a new formulation to compute self-potential signals associated with ground water flow, Hydrology and Earth System Sciences Discussions, 11(5), 1661-1671.

Doll, H. G., 1949, The SP log: theoretical analysis and principles of interpretation, Transactions of the AIME, 179(01), 146-185.

Eskola, L., 1992, Geophysical interpretation using integral equations, Springer Netherlands, London, Great Britian.

Finley, R. J., Speer, S. W., and Diecchio, R. J., 1984, Geology and Engineering Characteristics of Selected Low-permeability Gas Sandstones: A National Survey (Vol. 138), Bureau of Economic Geology, The University of Texas at Austin, USA.

Hill, H. J. and Millburn, J. D., 1956, Effect of clay and water salinity on electrocemical behavior of reservoir rocks, Transactions of the American Institute of Mining and Metallurgical Engineers, 207, 65-72.

Kerver, J. K. and Prokop, C. L., 1957, Effect of the presence of hydrocarbons on well logging potential, Fall Meeting of the Southern California Petroleum Section of AIME, 17-18 October, Los Angeles, California, Society of Petroleum Engineers.

McCall, C., Von Gonten, W. D., and Osoba, J. S., 1971, The effect of hydrocarbons on the SP opposite sands, Log Analyst, 12(06), 3-12.

Meunier, A., 2005, Clays, Springer Science and Business Media, Berlin, Germany.

Mounce, W. D. and Rust W. M., Jr., 1944, Natural potentials in well logging, Transactions of the AIME, 155(01), 49-57.

Poupon, A., Loy, M. E. and Tixier, M. P., 1954, A contribution to electrical log interpretation in shaly sands, Journal of Petroleum Technology, 6(6), 27-34.

Revil, A., 1999, Ionic diffusivity, electrical conductivity, membrane and thermoelectric potentials in colloids and granular porous media: a unified model, Journal of Colloid and Interface Science, 212(2), 503-522.

Salazar, J. M., Torres-Verdín, C., Alpak, F. O., Habashy, T. M., and Klein, J. D., 2006, Estimation of permeability from borehole array induction measurements: application to the petrophysical appraisal of tight gas sands, Petrophysics, 47(6), 527-544.

Tabanou, J. R., Glowinski, R., and Rouault, G. F., 1988, SP deconvolution and quantitative interpretation in shaly sands, Log Analyst, 29(5), 322-343.

Waxman, M. H., and Smits, L. J. M., 1968, Electrical conductivities in oil-bearing shaly sands, Society of Petroleum Engineers Journal, 8(02), 107-122.

Woodruff, W. F., Revil, A., Jardani, A., Nummedal, D., and Cumella, S., 2010, Stochastic Bayesian inversion of borehole self-potential measurements. Geophysical Journal International, 183(2), 748-764.

ABOUT THE AUTHORS

Joshua Bautista-Anguiano graduated from the National Autonomous University of Mexico in 2013 with his Bachelor's degree in Geophysical Engineering. He is currently pursuing his Ph.D. in Petroleum Engineering at The University of Texas at Austin and works as a graduate research assistant for the Joint Industry Research Consortium on Formation Evaluation. He is a 2015 SPWLA student member.

Carlos Torres-Verdín received a Ph.D. in Engineering Geoscience from the University of California at Berkeley in 1991. During 1991-1997, he held the position of Research Scientist with Schlumberger-Doll Research. From 1997-1999, he was Reservoir Specialist and Technology Champion with YPF (Buenos Aires, Argentina). Since 1999, he has been affiliated with the Department of Petroleum and Geosystems Engineering of the University of Texas at Austin, where he is currently Full Professor, holds the Brian James Jennings Memorial Endowed Chair in Petroleum Engineering, and conducts research on borehole geophysics, formation evaluation, well logging, and integrated reservoir characterization. Dr. Torres-Verdín is the founder and director of the Research Consortium on Formation Evaluation at the University of Texas at Austin, which is currently sponsored by 32 companies. He has published over 140 refereed journal papers and 180 conference papers, holds 2 patents, and has served as Guest Editor for Radio Science, as Associate Editor for the Journal of Electromagnetic Waves and Applications, SPE Journal, and *Petrophysics* (SPWLA). He is currently Assistant Editor for *Geophysics* and chair of the editorial board of *The Leading Edge* (SEG). Dr. Torres-Verdín is recipient of the 2014 Gold Medal for Technical Achievement from the SPWLA, of the 2006 Distinguished Technical Achievement Award from the SPWLA, of the 2008 Formation Evaluation Award from the SPE (Society of Petroleum Engineers), of the 2003, 2004, 2006, and 2007 Best Paper Awards in *Petrophysics* by the SPWLA, of the 2006 and 2014 Best Presentation Awards and the 2007 Best Poster Award by the SPWLA.